IEEE Access
Multidisciplinary | Rapid Review | Open Access Journal

Received August 12, 2021, accepted August 17, 2021, date of publication August 24, 2021, date of current version September 1, 2021.

Digital Object Identifier 10.1109/ACCESS.2021.3107421

Energy Efficient Torque Allocation Design Emphasis on Payload in a Light-Duty Distributed Drive Electric Vehicle

PRANJAL BARMAN[1] AND BRIAN AZZOPARDI[2], (Senior Member, IEEE)
[1]Department of Electronics and Communication Technology, Gauhati University, Guwahati, Assam 781014, India
[2]MCAST Energy Research Group, Malta College of Arts, Science and Technology (MCAST), Institute of Engineering and Transport, PLA9032 Paola, Malta

Corresponding author: Brian Azzopardi (brian.azzopardi@ieee.org)

This work was supported in part by the European Commission H2020 TWINNING Networking for Excellence in Electric Mobility Operations (NEEMO) Project under Grant 857484.

ABSTRACT Light-Duty Electric Vehicle (LDEV) with a distributed drive powertrain provides several potential advantages in terms of flexibility, controllability and responsiveness over conventional powertrains. The precise distribution of driving and braking torque of such configuration is crucially vital for improving the overall performance and efficiency of the vehicles. This paper proposes a new torque allocation (TA) model emphasizing the wheel load variation due to the passenger occupancy payload. A light-duty vehicle model is developed along with the occupancy payload arrangement and a dynamic tire-road friction estimation method for the control system for wheel slip. This proposed TA algorithm uses offline optimization to derive the necessary transmissible torque to the driving wheels. Unlike conventional optimization, it adopts a set of predefined distribution coefficients. Therefore it can execute in a real time platform without high computation power and additional hardware requirements. The efficiency of the model is analyzed using Indian Urban Drive Cycle (IN-UDC). A comparative analysis using a traditional torque allocation model highlights the contributions of this novel torque allocation. The results obtained from various simulations demonstrate the effectiveness of the proposed new TA algorithm.

INDEX TERMS Electric vehicle (EV), Indian urban drive cycle (IN-UDC), light duty electric vehicle (LDEV), torque allocation (TA).

I. INTRODUCTION

With the ever-increasing fuel crisis, thriving environmental consciousness and adverse effects of climate change, various automotive industries are taking more remarkable initiatives to develop eco-friendly vehicles that reduce the global carbon footprint [1]. As an outcome, Electric Vehicles (EV) have accelerated to fulfil these requirements worldwide. Meanwhile, the advancement of motor technology opened up several new possibilities to improve the existing EV powertrain concepts. The hybridization of EV powertrain configurations leads to new variances and possibilities that allow research in several new directions. Distributed drive-train is one kind of powertrain hybridization that has been evolving in recent years. This concept becomes widely popular in modern-day research and industrial perspectives. In a distributed drive powertrain configuration, the motors are attached to the wheels independently [2], [3]. Therefore, it offers much better design flexibility, controllability, responsiveness, safety and provides more opportunities to improve the control methodologies [4], [5]. Furthermore, the over-actuation features of a distributed drive train provides diverse control technologies such as Anti-Lock Braking System (ABS), Acceleration Slip Regulation (ASR)and Advanced Driver Assistance System (ADAS) [6]. Quite a few research works are available that deals with general studies on distributed drive EVs. The majority of the works are focused on improving dynamic performance and overall powertrain efficiency. It is worth mentioning that these improvements are mostly related to the torque allocation (TA) strategies. There are two TA strategies categories: (i) the equal torque distribution strategy and (ii) the real-time torque distribution strategy [7]. The former strategy dispatched the total torque evenly to each driving wheel. Therefore it intuitively represents a scenario in which all the driving wheels work in very similar dynamics and somehow resemble a generic motor. This approach

The associate editor coordinating the review of this manuscript and approving it for publication was Ton Duc Do.

essentially serves as a benchmark to assess the performance of the real-time torque distribution strategy in which torque distribution is non-uniform. In comparison, the real-time torque distribution strategy is more complicated in critical traffic conditions. Therefore, it is essential to investigate some adaptive control strategy that deals with the road-tire interactions to ensure better stability and driving comfort. Moreover, there have been significant opportunities to develop an efficient TA scheme for distributed drive-train configuration that helps to improve the vehicle energy economy shortly [8], [9].

A passenger vehicle comprises several components distributed within its exterior envelope. Therefore all the vehicle masses can resemble a payload located at its Center of Gravity (CG) [10]. The position of CG ideally is located where the longitudinal and lateral axis of a vehicle intersect with each other. However, in a practical vehicle, the location of CG may be deviated from its ideal location due to the asymmetric distribution of sprung mass. The deviation of CG becomes more significant if the vehicle curb mass is low, such as in a Light-Duty Electric Vehicle (LDEV).The sprung mass of a passenger vehicle is contributed by passenger or cargo weight. Therefore the position of CG in the case of LDEV, may significantly be influenced by the passenger or cargo payload [11]. The deviation of CG for its ideal location is proportional to that of the passenger to curb weight ratio of a vehicle. Table. 1 lists the passenger to curb weight ratio of some commercially available vehicles. As a result of the CG shift, the reaction force experienced by each driving wheel changes drastically. Consequently, the position of CG significantly influences the torque responsible for the longitudinal movement of the vehicle. Therefore, analysis of the torque allocation (TA) model relying on the occupancy or cargo payload is crucial for improving of overall vehicle efficiency. Moreover, to ensure the higher efficiency of an LDEV, it is indispensable to search for a new TA method that reduces the motor power loss by precisely allocating the driving torque among the wheels [12].

TA strategies in the literature discussed the improvement of EV efficiency. Table. 2 summarises few investigations of the existing literature. Suzuki *et al.* developed a force distribution strategy to minimize tire energy loss to improve total drive efficiency [13]. Although effective, the practical implementation of this strategy requires more advanced tyre state estimators. Wang *et al.* developed an optimal torque allocation strategy without analyzing the torque distribution as a function of vehicle speed and torque demand [14]. The approach is also limited to some specific powertrain configurations.

Fujimoto and Harada proposed a driving and braking force distribution based on slip ratio and motor loss calculations [15]. Despite having several advantages, their approach lacks in providing the results of high-speed operations. Furthermore, the proposed strategies in [1], [16], and [17] are found efficient and straightforward compared to torque-fill control for multi-speed transmission systems adopted in [9].

TABLE 1. Passenger to Curb Weight Ratio (PCWR) of commercial available LDEVs (average weight of a passenger is considered 70 kg).

LDEV	Passengers	Curb weight (kg)	PCWR	PCWR (driver only)
BYD e6	5	2020	0.173	0.035
Tesla S60	5	1961	0.178	0.035
Tesla S40	5	1850	0.189	0.038
Ford Focus	5	1674	0.209	0.042
Chevrolet Bolt	5	1624	0.216	0.043
Renault Fluence	5	1543	0.227	0.045
Nissan Leaf	5	1521	0.230	0.046
Renault Zoe	5	1468	0.238	0.047
Mercedes Benz	5	1445	0.242	0.048

Zhang *et al.* proposed a robust control scheme to improve the lateral stability of a four in-wheel drive vehicle. They have achieved high precision reference tracking and guaranteed smooth control action by adopting a robust sliding mode controller [18]. Wang *et al.* presented the comprehensive experimental performance and energy efficiency characterizations of an independent-wheel-drive electric-ground-vehicle. Their work greatly improved the operational energy efficiency by utilizing actuation flexibility [14]. Same group presented a synthesized control allocation of sliding mode control (SMC) and adaptive energy-efficient control to achieve optimal energy efficiency of an electric ground vehicle [16], [19]. Within the aforementioned approaches, a few performs reasonably well under certain constraints. However few dynamic parameters such as vehicle centripetal force and passenger payload is ignored in the optimal solution. In addition to that, some of the existing methods avoid the discussions of the strategies that either consider the comprehensive model for wheel torque distribution or algorithm that can be easily implemented for real-time applications. Considering these limitations, in this work, we have addressed a simple, tunable and effective solution for TA design that improves the overall vehicle efficiency.

In contrast to the work cited above, the novelty of the presented work lies in developing a new TA model that considers passenger occupancy payload, road-tire interaction and vehicle dynamics. This work focuses on an LDEV with a rear wheel distributed drive powertrain. This powertrain configuration provides flexibility to improve drive efficiency under various operating conditions. The proposed TA algorithm uses an offline optimization process to develop the necessary transmissible torque for each driving wheel. The discontinuous optimization problem adopts the Genetic algorithm, which does not rely on hypothetically predicted initial values. Unlike the conventional optimization method, the proposed TA is set with predefined distribution coefficients. In practice, the proposed TA may can be embedded in the LDEV controller in the form of a look-up table. Hence it can execute in a real-time platform without the requirement of high processing power and additional hardware units.

TABLE 2. Summary of EV TA strategies.

EV Model	Features	Advantages	Limitations
Four-wheel drive [9]	Compensation of the torque gap using a torque-fill controller that changes the motor torque by avoiding the active axle during a gearshift	Improves the energy efficiency for the specific wheel torque-speed	System complexity, cost, and mass
Drive-by wire [13]	Minimization of tyre workload as well as energy dissipation during the slip	Effectively minimized the tyre workload and improving vehicle stability	Practical implementation requires advanced tyre model estimators
Independently actuated in the wheel [14]	Experimental characterization of motor torque responses, power consumption and efficiency during driving and regenerative braking	Improves the vehicle efficiency	Configuration specific and the method avoids the desired speed torque demand
Four in-wheel motor [15]	Optimizes the driving and braking force using wheel slip	Minimizes energy consumption and optimizes the torque distribution ratio	Results limited at low speed over the straight road
Four in-wheel motor [16]	Optimal operating point selection using adaptive convergence method	Better performance compared to the traditional method	Trade-off between the vehicle stability and energy optimization
Four-wheel drive [17]	Offline optimization process	Simple and efficient	Effective in low torque demand

The efficiency of the LDEV is analyzed using Indian Urban Drive Cycle (IN-UDC).

The rest of the article is organized as follows. Section. II describes the vehicle structure and passenger payload model and brief introduction of motor, battery and tire model. Then Section. III presents the torque allocation system design. Section. IV discusses the slip control method presented in work. The simulation model is presented in Section. V. Section. VI discusses the results obtained and finally in Section. VII, the main conclusions and key findings distinctive from previous studies are presented.

II. SYSTEM MODELLING

A. VEHICLE STRUCTURE AND OCCUPANCY PAYLOAD MODEL

The geometry of the proposed vehicle is shown in Fig. 1(a) and the major dimensions are tabulated in Table. 3. Fig. 1(b) presents the seat locations along with the chassis geometry. The ideal position of CG is considered at (0,0), the point which is symmetrical about the longitudinal and lateral centre plane of the vehicle. Then a set of possible occupancy combinations are assumed for detailed theoretical analysis illustrated in Fig. 1(c). Accordingly the shift of CG for the assumed combinations are plotted concerning the ideal location (0,0) in Fig. 1(d). The shift of CG results in an uneven distribution of reaction forces experienced by each wheel of the vehicle. It is worthnoting that the distribution ratio of the wheel reaction forces is inversely proportional to that of the curb mass of the vehicle. Hence, the significance of the presented analysis is more noteworthy in the case of LDEVs. The reaction force (or normal force) experienced by each wheel can be obtained by defining the position of CG using Eq. 1.

$$\overline{X} = \frac{\sum m_p x_p}{M + \sum m_p}; \quad \overline{Y} = \frac{\sum m_p y_p}{M + \sum m_p}; \tag{1}$$

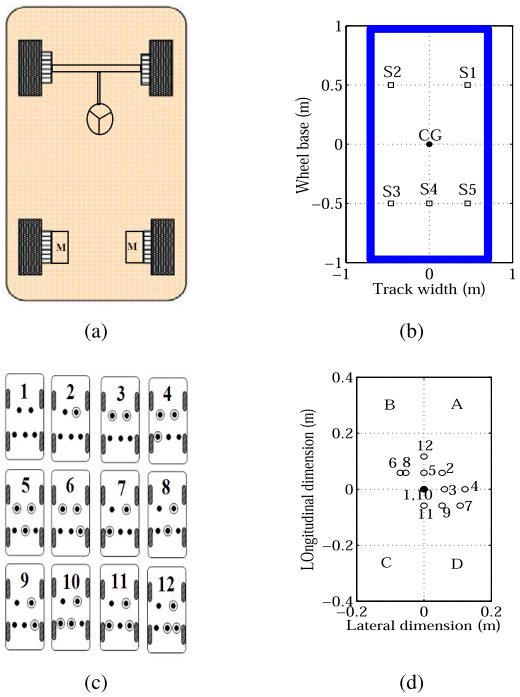

FIGURE 1. (a) Distributed drive EV architecture, (b) Seating geometry of the proposed vehicle, (c) Occupancy payload combinations assumed for this analysis where encircled dots represent the occupied positions, (d) Shift of CG due to the occupancy payload combinations.

TABLE 3. Vehicle dimensions.

Symbol	Parameter	Quantity
l	Wheel base	1950mm
b	Track width	1240mm
r	Wheel radius	330mm
M	Curb weight	500kg
m_p	Passenger weight	$70kg$

Here $\overline{X}$ and $\overline{Y}$ are the lateral and longitudinal position coordinates of the CG, m mass of individual passenger or cargo, p number of passenger and M mass of the vehicle.

The reaction force exerted on each wheel of a symmetric vehicle can be given as in [10]

$$F_{Zij} = \frac{1}{2}F_{Z0} \pm \Delta F_Z \tag{2}$$

Here F_{Zij}: wheel reaction force, i: 1 for the front, i: 2 for the rear, j: 1 for left, j: 2 for right, F_{Z0}: wheel reaction force of the unloaded vehicle, ΔF_z: change in wheel load due to the shift of CG. The $\pm$ operation depends on the quadrants across which the direction of CG shifted. The quadrants are indicated as A, B, C and D as shown in Fig. 1(d). The ΔF_Z could also be due to other asymmetric reasons such as engine torque, acceleration and road irregularities. However in this work, we have ignored the other reasons for the ease of analysis. Here we have considered both static and dynamic states of the vehicle. The vehicle is parked over different road surfaces in static conditions and accelerates in dynamic conditions. In both cases, the wheel reaction forces determine CG shift due to the passenger occupancy combinations. Accordingly, the necessary tractive efforts are evaluated for the TA design.

In static condition the vehicle is parked on a level road. In such a situation, the wheel reaction force experienced by the driving wheels can be defined by Eq. 3 [10].

$$F_{Zij} = Mg\frac{l/2}{l}\frac{b/2}{b} = \frac{1}{4}Mg \tag{3}$$

Here, g-acceleration due to gravity, l-wheel-base, b-track-width. It is seen that the reaction force will be shared uniformly among the four wheels, if the vehicle weight distribution is uniform. However, in a practical scenario, the position of CG will be located over a region neighbourhood of the coordinate (0, 0) which can be defined by $(\overline{X}, \overline{Y})$. Now we can modify Eq. 3 as:

$$F_{Zsij} = \frac{1}{4}Mg\frac{(\frac{l}{2} \pm \overline{X})}{l}\frac{(\frac{b}{2} \pm \overline{Y})}{b} \tag{4}$$

In the following case, if the car is speeding with acceleration a on the level pavement then, the reaction forces experienced by rear wheels to be increased. Therefore, an additional term will be added to Eq. 4 to complete the analytical model. This has been indicated by F_{Zdij} and can be derived as:

$$F_{Zdij} = \frac{1}{4}Mg\frac{(\frac{l}{2} \pm \overline{X})}{l}\frac{(\frac{b}{2} \pm \overline{Y})}{b}\frac{ha}{lg} \tag{5}$$

Thus the total force on each rear wheel is the summation of the static and dynamic component force under the influence of the passenger occupancy or cargo in Eq. 6.

$$F_{Zij} = F_{Zsij} + F_{Zdij} = \frac{1}{4}Mg\frac{(\frac{l}{2} \pm \overline{X})}{l}\frac{(\frac{b}{2} \pm \overline{Y})}{b}(1 + \frac{ha}{lg}) \tag{6}$$

where, h: denotes the height of the CG. Eq. 6 describes the static and dynamic model of the wheel reaction force under the influence of the passenger occupancy or cargo.

Now if the vehicle is accelerating over a banked road [20] with slope β, then the reaction force of the rear wheel can be given as:

$$F_{Zij} = \frac{1}{4}Mg\frac{(\frac{l}{2} \pm \overline{X})}{l}\frac{(\frac{b}{2} \pm \overline{Y})}{b}(cos\beta - \frac{h}{b}sin\beta + \frac{ha}{lg}) \tag{7}$$

$$F_{Zij} = \frac{1}{4}Mg\frac{(\frac{l}{2} \pm \overline{X})}{l}\frac{(\frac{b}{2} \pm \overline{Y})}{b}(cos\beta + \frac{h}{b}sin\beta + \frac{ha}{lg}) \tag{8}$$

Next, we have to consider the car that is accelerating over an inclined surface. This condition increases the wheel reaction force experienced by each rear wheel. Subsequently the reaction force experienced by each front wheel will decrease. The change of the wheel reaction force is a function of the road grade angle θ and the acceleration a. In the inclined surface, we have ignored the analysis of a static vehicle because the probability of a car parked over an inclined surface is very rare in general. The wheel reaction forces due to the influence of road inclination can be given as:

$$F_{Zij} = \frac{1}{4}Mg\frac{(\frac{l}{2} \pm \overline{X})}{l}\frac{(\frac{b}{2} \pm \overline{Y})}{b}(cos\theta - \frac{h}{l}sin\theta - \frac{ha}{lg}) \tag{9}$$

$$F_{Zij} = \frac{1}{4}Mg\frac{(\frac{l}{2} \pm \overline{X})}{l}\frac{(\frac{b}{2} \pm \overline{Y})}{b}(cos\theta + \frac{h}{l}sin\theta + \frac{ha}{lg}) \tag{10}$$

The analysis over the road surface having crest and dip is also essential for off-road driving conditions. The crest is an outward curvature, and the dip is an inward curvature of a road surface. These occur due to road deformities or under the influence of speed breakers or due to some similar obstacles. Such deformities have a significant effect on the wheel reaction force. When a vehicle moves over a crest surface or a convex curve, the wheel reaction force will decrease compared to the force over a flat surface. This condition is due to the development of the centrifugal force in the vertical direction. If we consider a crest with a radius of curvature r_c, then the wheel reaction force can be derived by Eq. 9 and Eq. 10 as:

$$F_{Zij} = \frac{1}{4}Mg\frac{(\frac{l}{2} \pm \overline{X})}{l}\frac{(\frac{b}{2} \pm \overline{Y})}{b}(cos\theta - \frac{h}{l}sin\theta - \frac{ha}{lg}) - F_{Zc} \tag{11}$$

Here F_{Zc} is the inward centrifugal force developed along the z-direction which can be expressed as:

$$F_{Zc} = \frac{1}{4}M\frac{v^2}{r_c}\frac{(\frac{l}{2} \pm \overline{X})}{l}\frac{(\frac{b}{2} \pm \overline{Y})}{b} \tag{12}$$

The Eq. 11 represents the wheel reaction force of the front wheel of a cresting vehicle. The wheel reaction force of the rear wheel can be represented by:

$$F_{Zij} = \frac{1}{4}Mg\frac{(\frac{l}{2} \pm \overline{X})}{l}\frac{(\frac{b}{2} \pm \overline{Y})}{b}(cos\theta - \frac{h}{l}sin\theta + \frac{ha}{lg}) - F_{Zc} \tag{13}$$

Now if the vehicle moves over a concave surface or a dip inward curvature, then the wheel reaction force will increase due to the development of centrifugal force opposite to the

vertical direction. F_{Zd} represents the additional force for dip surface with a radius of curvature r_d in [10]

$$F_{Zd} = \frac{1}{4}M\frac{v^2}{r_d}\frac{(\frac{l}{2} \pm \overline{X})}{l}\frac{(\frac{b}{2} \pm \overline{Y})}{b} \tag{14}$$

Then the expression that represents the wheel reaction force of a dipping vehicle can be written as:

$$F_{Zij} = \frac{1}{4}Mg(\frac{(\frac{l}{2} \pm \overline{X})}{l}\frac{(\frac{b}{2} \pm \overline{Y})}{b}cos\theta - \frac{h}{l}sin\theta) - Ma\frac{h}{l} + F_{Zd} \tag{15}$$

$$F_{Zij} = \frac{1}{4}Mg(\frac{(\frac{l}{2} \pm \overline{X})}{l}\frac{(\frac{b}{2} \pm \overline{Y})}{b}cos\theta - \frac{h}{l}sin\theta) + Ma\frac{h}{l} + F_{Zd} \tag{16}$$

Eq. 15 and Eq. 16 represents the reaction force experienced by front and rear pair of wheels on a dip surface.

To develop the proposed model, a comprehensive study of the vehicle longitudinal dynamics is essential. Therefore we have considered the total driving force requirements during a longitudinal acceleration of a vehicle that is derived in Eq. 17.

$$F_{Tx} = C_{rr}F_Z + F_Z sin\phi + F_Z a_{max} + F_{drag} \tag{17}$$

where the first term represents the rolling resistance force and C_{rr}-rolling friction coefficient, the second term represents grade force and ϕ-grade angle, the third term represents the acceleration force and a_{max}-maximum acceleration of the LDEV and last term represents the aerodynamic drag force [21]. Here, and. In this analysis, twelve different passenger payload combinations are assumed to derive the tractive effort where the driver seat $S0$ is always occupied except for the no loading condition. The rest of the four seats are occupied in a sequence presented in Fig. 1(c).

In the proposed EV model, the driving wheels are the rear wheels and the front wheels are passive wheels. Hence the longitudinal tractive torque is shared equally by two wheels in the absence of passenger or cargo. Therefore each driving torque can be expressed in Eq. 18.

$$T_{xi} = \frac{1}{2}F_{Tx} \times r \tag{18}$$

where r indicate the wheel's rolling radius, $i = 1, 2$ for the rear left and rear right wheel. The tractive torque of both rear wheels under the influence of the six payloads mentioned above is presented in Fig. 2. Here, out of the twelve possible combinations, six most widely occurred occupancy instances are used those are numbered as 4, 5, 6, 10, 11 and 12 in Fig. 1(c). Fig. 2 evinces the uneven torque experience among the driving wheels due to the effect of passenger payload variations. This essentially require a TA model to deal with the torque non-uniformity.

B. ELECTRIC MOTOR

In the proposed LDEV, each rear wheel is independently equipped with the DC motor through a reduction gear. This configuration is widely accepted in distributed powertrain design. The DC motor acquires its popularity due to several

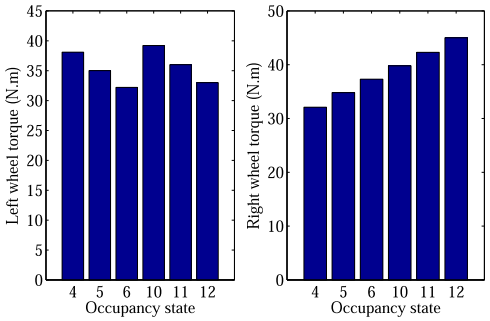

FIGURE 2. Tractive torque under the influence of few occupancy payload combinations mentioned in Fig. 1(c).

merits such as simple control, wide speed-torque range, linearity among speed-torque and applied voltage, compact size and high power efficiency [22]. It is a well-known fact that the induction motor (IM) or Brush-Less-DC motors (BLDC) have some superior advantages compared to DC motors in terms of power density and maintenance. However, the low and medium power propulsion applications (e.g. Neighbourhood Electric Vehicle (NEV)), the DC motors are still popular because of their technical maturity, simple control and cost-effectiveness [23]. Moreover, the complicated control strategies in IM or BLDC motors make the control system more expensive than the DC motors. Therefore, for analytical simplicity, we have adopted DC motor in this work. The DC motor model is described by Eq. 19.

$$E = R_a i + L_a\frac{di}{dt} + E_b \tag{19}$$

where E- applied voltage, i-motor current, R_a- Armature resistance, L_a- Armature inductance and E_b- Back emf constant. The other parameters can be defined as

$$E_b = K_b\omega_m \tag{20}$$

$$T_m = K_t i \tag{21}$$

Moreover, the motor voltage and current is always limited to

$$E \leq E_{max}, i \leq i_{max} \tag{22}$$

The motor power is a function of the output torque, speed and motor efficiency during driving, thus yields

$$P_m = \frac{\pi T_m \omega_m}{30\eta} \tag{23}$$

Here P_m-motor power and η-efficiency. The motor efficiency η can be looked up from the motor efficiency map shown in Fig. 3. To determine the motor efficiency, we have to use the torque-speed characteristics data from a practical PMDC motor of $1HP$ power rating. The details of the motor characteristics evaluation process had been presented in a previously published work given in [24]. The core part of the work involved a gear-belt mechanism to apply the necessary torque, speed sensor to calculate the motor speed and DC-DC converter to change the applied voltage. Accordingly the

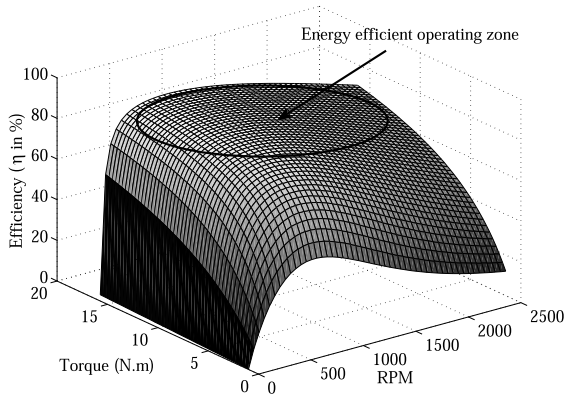

FIGURE 3. Motor efficiency map with the optimal operating region.

efficiency expression of the motor is calculated using a curve-fitting tool. Finally the efficiency map is derived with the help of Eq. 24.

$$\eta = \frac{T_i\omega_i}{T_i\omega_i + T_i^2K_c + \omega_iK_f + \omega_i^3K_\omega + c} \tag{24}$$

The contour efficiency values to be adopted to the proposed TA are shown in the encircled region in Fig. 3.

C. BATTERY MODEL

In the proposed vehicle model, the lead-acid battery package is used as the primary source. The lead-acid technology is very useful in low-cost vehicles in terms of cost to energy ratio. However, these batteries show relatively low cycle life compared to other secondary batteries. Therefore efficiency calculation and understanding of charging-discharging cycles is very crucial. One of the well-established models for battery charging-discharging analysis is the Shepherd model, which is based on the electrochemical behaviour directly in terminal voltage, open-circuit voltage, internal resistance, discharge current and state-of-charge. The discharge model for the lead-acid battery is as in [25]

$$V_{batt} = E_0 - Ri - K\frac{Q}{Q - it}(it + i^*) + e^t \tag{25}$$

Here V_{batt}-battery voltage, E_0-battery constant voltage, R-internal resistance, K-polarization constant, Q-battery capacity, i-battery current and i^*-low frequency current dynamics. In this work, the battery model input is the power demand to the drive motors and outputs are the voltage, current and depth-of discharge (DOD) value. It is worth noting that the DOD of a typical lead-acid battery is below 50%.

D. TIRE MODEL

A tire model describes the relationship between tire parameters, tire states and tire forces which can estimate the road-tire friction coefficient. We have adopted the Brush model [26] because it utilizes fewer parameters than other established methods like the Magic formula or linear tire model. Besides that, the Brush model considers the effect of friction and non-linearity during increased slip angle. In a pure longitudinal slip case, the tire longitudinal force F_{Tx}, can be represented as [26]

$$F_{Tx}(\lambda, \mu) = 3\mu F_Z\theta_x\sigma_x\{1 - |\theta_x\sigma_x| + \frac{1}{3}|\theta_x\sigma_x|^2\}; for \lambda \leq \lambda_d \tag{26}$$

$$= \mu F_Z sign(\lambda); for \lambda > \lambda_d \tag{27}$$

Here λ-slip ratio, μ-friction coefficient and λ_d-slip limit. The other parameters are defined in Eq. 28 and Eq. 29.

$$\theta_x = \frac{2C_pl^2}{3\mu F_Z} \tag{28}$$

$$\sigma_x = \frac{\lambda}{\lambda + 1} \tag{29}$$

Here, the C_p-stiffness coefficient of tire tread and l-half of the tire contact length. Here we have considered the model input is the power demand to the drive motors and outputs are the longitudinal slip value of the respective wheel.

III. TORQUE ALLOCATION DESIGN

The simplified vehicle control diagram is shown in Fig. 4. Two identical DC motors are independently mounted in each rear wheel of the vehicle. The motors are driven by two independent DC-DC converters having appropriate specifications.

It is significant for an optimal TA design to analyze the LDEV's power consumption for various driving cycles. If the driving torque is distributed among the motors according to the vehicle working conditions, then the efficiency of the vehicle is highly improved. For these conditions, the objective function of motor power from [1] is:

$$minJ_d = \sum P_{mi} = \sum \frac{\pi T_{mi}\omega_{mi}}{30\eta(T_m, \omega_m)} \tag{30}$$

The objective function subjects to the following equality constraints and inequality constraints:

$$\sum P_{mi} = T_d; \quad \sum T_{mi} \geq T_{mfl} + T_{mfr}; \tag{31}$$

$$T_{mi} \leq T_{max}; \quad \omega_{mi} \leq \omega_{max} \tag{32}$$

where T_d is the torque demand, T_{max} represents the motor torque limit and ω_{max} is the maximum wheel speed in rpm. Assumptions are taken to simplify the calculations and easy real-time performance of TA. Firstly, the drive motors have identical torque-speed characteristics. Secondly, the drive line components of LDEVs such as motors, batteries and control circuits are distributed so that the CG is located at its ideal position when unloaded. Subsequently, on a typical urban driving cycle the speed of each wheel is approximately equal at the straight road as the longitudinal wheel slip ratio usually maintains below 0.1 on urban road. These assumptions can be formulated as Eq. 33. Here p represents the optimal torque distribution coefficient. Finally, the objective

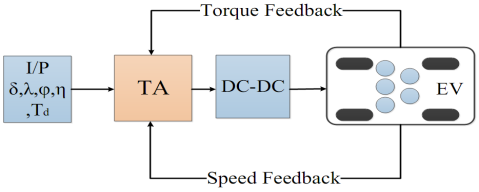

FIGURE 4. Vehicle control structure.

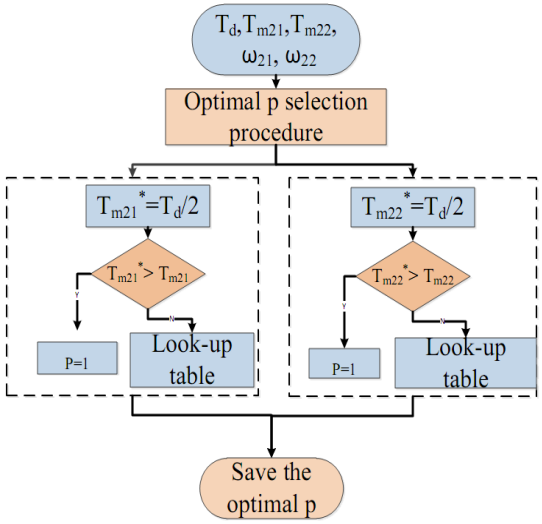

FIGURE 5. Algorithm to determine optimal torque distribution coefficient.

function of power consumption for the driving condition is expressed by Eq. 34.

$$T_{m1} = T_{m2} = p\frac{T_d}{2} \tag{33}$$

$$minJ_d = \sum \frac{\pi p T_d \omega_{mi}}{60\eta(p\frac{T_d}{2}, \omega_m)} \tag{34}$$

In this study, we have used genetic algorithm for natural selection to solve discontinuous constraint objective function. The main advantage of the genetic algorithm is that it effectively prevents the local optimization problem and acquires the solution accurately and rapidly. The calculations are performed using the global optimization toolbox in the dedicated simulator. Global optimization-based control allocation methods have been effectively used to solve the equivalent nonlinear allocation problems [27]. The solution of the aforementioned objective function is given as a two-dimensional lookup table with the desired driving torque-speed range. This approach avoids numerous online computations and mitigates the requirements of real-time implementation. The algorithm to determine the optimal torque distribution coefficient is shown in Fig. 5. The schematic of the proposed TA strategy is shown in Fig. 6. The optimal torque distribution coefficient is obtained as the output value through look-up table and interpolation as illustrated in Fig. 7. In this system the speed of the drive motors at various cornering manoeuvres are controlled by the steering angle based electronic

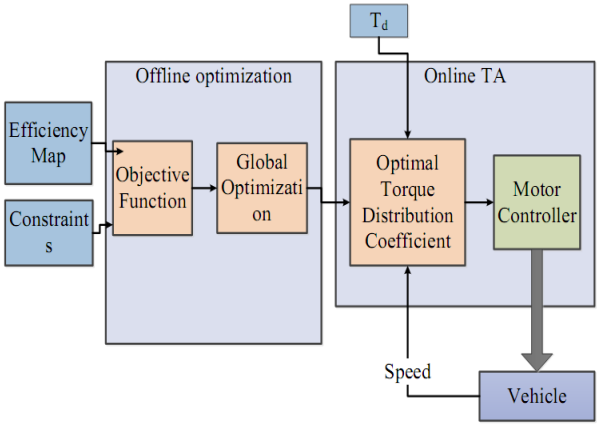

FIGURE 6. Proposed TA scheme.

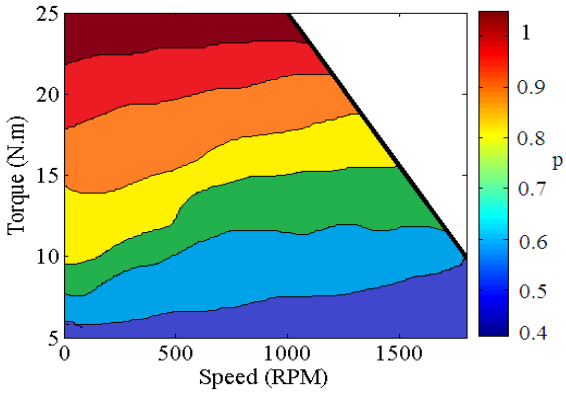

FIGURE 7. Optimal torque distribution coefficients.

differential as explained in [3] and [28]–[30]. It is noted that, due to the limited scope of the presented work, the cornering performances of the LDEV are not presented explicitly.

IV. SLIP CONTROL METHOD

The study of a dynamic vehicle's road-tire-interaction behaviour is essential for the development of a slip control system. The dynamic friction coefficient is an important variable for the vehicle designers to develop electronic stability control, ABS or cruise control [31]. However, acquiring the knowledge of road tire friction coefficient in an actual vehicle is not very straightforward. Despite the difficulties, researchers have proposed several innovative ideas to estimate the road-tire friction coefficient. This article has adopted a friction estimation method from work presented in [32]. The method deals with the estimation of road-tire friction coefficient with the help of the existing friction map. Based on the estimated friction coefficient, a reference slip ratio is determined and then the motor torque output has been limited by allowable torque value. A novel $(\mu-\lambda)$ curve based on five existing road conditions is confirmed in this method. Then the peak value of μ has been traced out and necessary slip control system is developed. In this work, we have used the

TABLE 4. Tire model parameters for various surface conditions.

Surface	a_1	a_2	a_3
Dry asphalt	1.28	23.9	0.52
Wet asphalt	0.86	33.8	0.35
Dry concrete	1.19	25.2	0.53
Snow	0.2	94.1	0.06
Ice	0.05	306	0

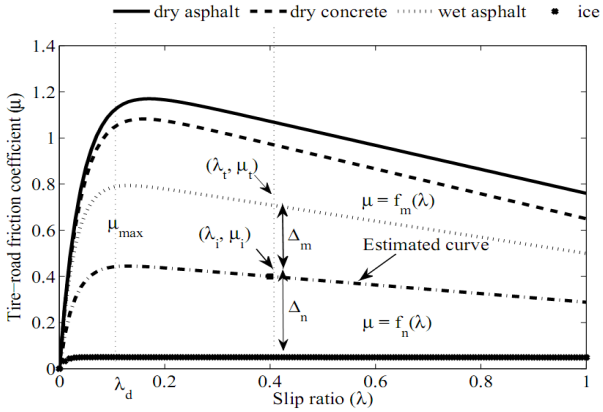

FIGURE 8. Slip estimation method from known friction map.

Burckhardt model for longitudinal $(\mu-\lambda)$ relationship which is given in [10] as:

$$\mu(\lambda) = a_1(1 - e^{-a_2\lambda}) - a_3\lambda \tag{35}$$

$$\lambda = -\frac{v - r\omega}{v} \tag{36}$$

The parameters a_1, a_2, a_3 for different road surfaces are mentioned in Table. 4. In this work, five most commonly available road surface conditions are put forward to estimate a workable slip value. Here the slip information λ is obtained from the ratio of wheel speed and vehicle speed using Eq. 36. With the use of λ, the instantaneous value of μ has been acquired by using Eq. 35 and accordingly a series of error values Δ_m, Δ_n is determined, as depicted in Fig. 8. Then the smallest error value has been used to formulate a new relationship as given by:

$$\mu(\lambda) = \frac{\Delta_n}{\Delta_m + \Delta_n} f_m(\lambda) + \frac{\Delta_m}{\Delta_m + \Delta_n} f_n(\lambda) \tag{37}$$

Eq. 37 signifies the estimated $(\mu - \lambda)$ curve at any instantaneous wheel slip. Using this value, the maximum tire-road friction coefficient can be expressed from Fig. 8 as:

$$\mu_{max} = f(\lambda_d) \tag{38}$$

It is worth mentioning that the point (λ_d, μ_{max}) is the peak value of the instantaneous $(\mu - \lambda)$ curve.

To highlight the effectiveness of the slip control method, we have conducted a simulation for the analysis of the Double-Lane-Changing (DLC) performance of the vehicle. Hence, we have to rely on a few assumptions to emulate the behaviour of the DLC experiment [33]. The assumptions of our simulation are 1) The left wheel of the vehicle experiences a slippery surface after travelling from a dry surface, 2) The right wheel is travelling on the dry surface throughout the simulation and 3) The slip control mechanism is activated based on the slip feedback received from lowest traction wheel.

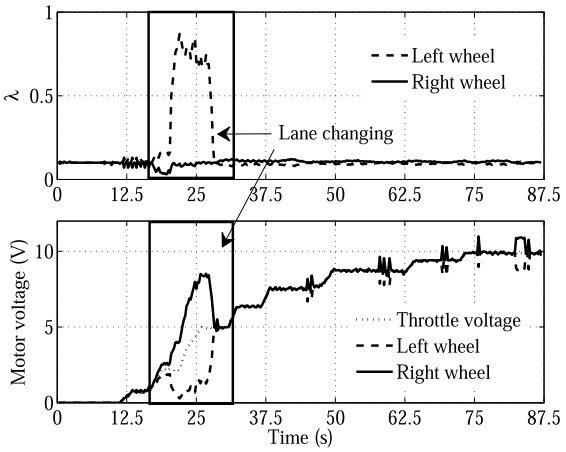

FIGURE 9. Simulation results for the validation of slip control method during Double Lane Changing (DLC) situation.

The simulation results are presented in Fig. 9. Here the wheel slip ratio λ and motor applied voltage are plotted during a straight driving trip. In this simulation, the acceleration level is increased gradually in a linear fashion. The left wheel of the vehicle is then experienced a slippery surface at 13 seconds and continues to slip upto 31 seconds which is indicated by a rectangle shown in Fig. 9. During this time-frame, the left wheel slip increases significantly and accordingly the slip control system is activated. Consequently, the motor voltage of the left wheel is decreased upto the desired level to limit the wheel slip. At the same time, the motor voltage of the right wheel is increased to deliver the necessary wheel torque to balance the vehicle. Once the vehicle overcomes the slippery surface, the TC system is deactivated and the vehicle control system usually functions.

V. MODEL SIMULATIONS

The proposed TA is examined in a software simulation environment with the necessary constraints for the vehicle geometry. The identical DC motor characteristic parameters are evaluated in the previous work [24]. The motor parameters used in the simulation are listed in Table. 5. The TA algorithm alters the motor operating region by maximizing the efficiency at the desired speed torque demand via optimal torque distribution coefficient. In practice, TA determines the motor operating region from the motor efficiency map in a look-up table as explained before. To highlight the effectiveness of the TA algorithm, the conventional torque distribution (CTD) approach is considered to evaluate the comparative analysis. In conventional traction systems, the gearing mechanism applies the same torque to both the traction wheels for all the vehicle trajectories independent of wheel speeds [34].

TABLE 5. Motor parameters.

Parameter	Value
P_{max}, V_{DC}, RPM	$1HP, 24V, 2500$
R_a	$150 \times 10^{-3}\Omega$
L_a	$230 \times 10^{-6}H$
f	$8kHz$
Inertia	$3.1kgm^2$
Viscous friction	$0.08N/ms$
Copper loss coefficient (K_c)	0.015
Iron loss coefficient (K_f)	1.2×10^{-3}
Windage loss coefficient (K_ω)	10^{-6}
Constant (c)	500

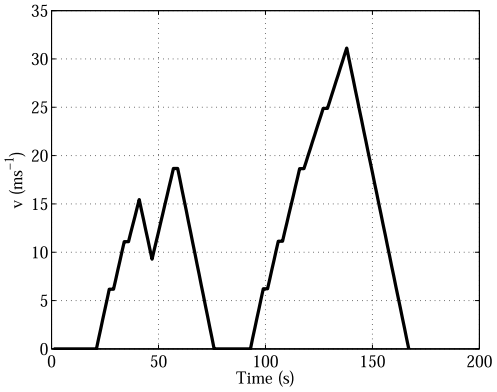

FIGURE 10. Indian Urban Driving Cycle (IN-UDC).

This can essentially serve as the benchmark to assess the performance of the real-time TA strategy [7]. The advantage of such traction is that if one wheel stops rotating or running freely because of slippery road conditions, the other wheel will accelerate up to twice the reference speed. However, this situation might create troubles for the motor windings and hence torque limiter is obligatory. Furthermore, during the cornering manoeuvres in a good road adhesion condition, the inner wheel produces an opposite moment to turn the vehicle. As a consequence, the steering becomes hard and vehicle energy losses increased subsequently. Moreover, it limits the maximum transmissible torque when the wheel is under slip. The works presented in [30], [35], and [36] adopted the CTD approach to control the vehicles.

Furthermore, to address the vehicle's overall efficiency of the vehicle, Indian Urban Driving Cycle (IN-UDC) is adopted into the model simulation. The IN-UDC is shown in Fig. 10, which involves a wide range of velocity information of Indian urban driving conditions. The efficiency of the LDEV with IN-UDC is examined merely by evaluating motor power consumption and efficiency. It is essential to mention here that, all the simulations are conducted over the level road acceleration with minimum road grade. Out of the twelve occupancy payload combinations (see Fig. 1(c)), only six most widely occurred occupancy instances have been chosen for simulation. Due to the CG shift the wheel reaction force

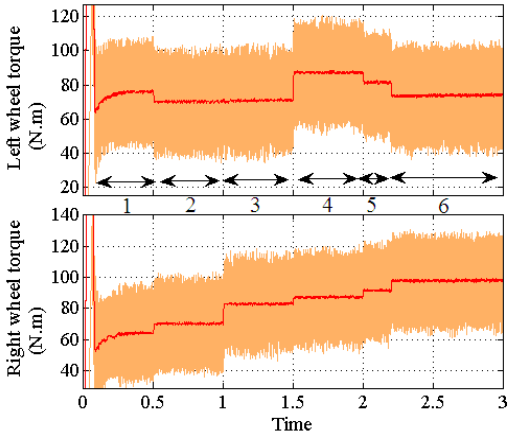

FIGURE 11. Motor torque using TA.

is considered to have a step change during the simulation. In addition to that, we have assumed that the occupancy payload combinations are changing while the simulation runs for a particular drive cycle. Furthermore, to evaluate and compare the performance of these two approaches mentioned above, the following assessment criteria are introduced:

1) Traction efficiency η_{tr}, which is defined as the ratio of theoretical energy consumption (E_t) to the actual energy consumption (E_a).

$$\eta_{tr} = \frac{E_t}{E_a} \times 100\% \tag{39}$$

2) The percentage change of the efficiency.

$$\%\eta_{ch} = \frac{\eta_{higher} - \eta_{lower}}{\eta_{higher}} \times 100\% \tag{40}$$

The simulation model validates the efficiency improvements of the proposed TA method in comparison to the CTD strategy.

VI. RESULTS AND DISCUSSIONS

Several simulations exploited the potential merits of the proposed method. The torque distribution using TA method are illustrated in Fig. 11. In this simulation, all the passengers described above occupancy combinations (from Fig. 1(c)) are evaluated over a continuous time scale. However, in a practical scenario, this analysis could be difficult for the whole set of combinations at a time. The results show that the torque allocation to each driving wheel for different occupancy combinations are unevenly distributed. A similar analysis is carried out by adopting the CTD approach having a similar simulation setup. The results obtained from CTD approach are shown in Fig. 12. Unlike TA, the results obtained from CTD method are essentially identical for both the drive motors. That means, due to the lack of adequate torque allocation capability,the CTD approach is less efficient compared to that of the TA approach. The initial SOC of the batteries is set at 80%. The motor efficiency by adopting the TA method is presented in Fig. 13.

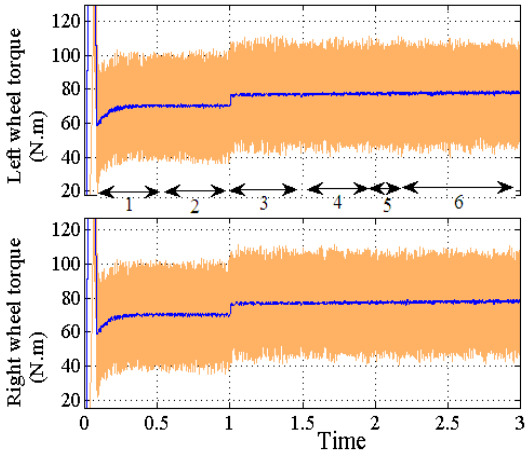

FIGURE 12. Motor torque using CTD.

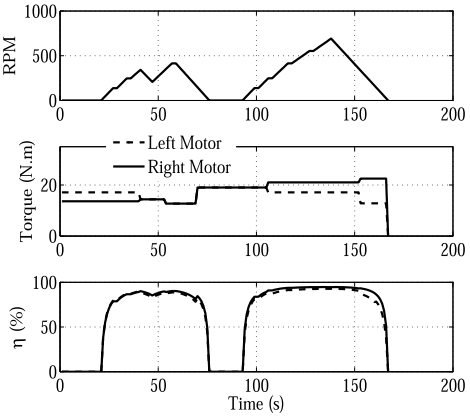

FIGURE 13. Motor efficiency at IN-UDC using TA.

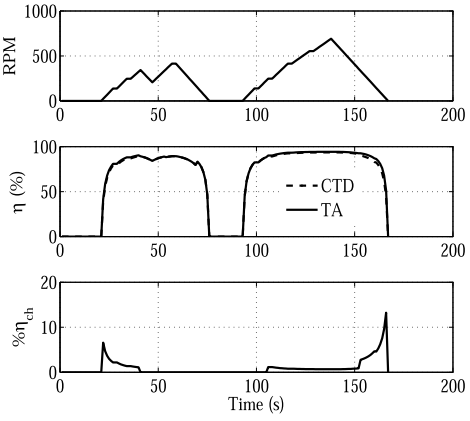

FIGURE 14. Efficiency comparison using TA and CTD method.

It is observed that the right motor is operated in a higher efficiency region compared to that of the left motor for the given occupancy payload instances. Fig. 14 indicates that the traction power efficiency is more than 10% when TA is applied compared to CTD. The motor power consumption for the complete driving cycle is shown independently in Fig. 15.

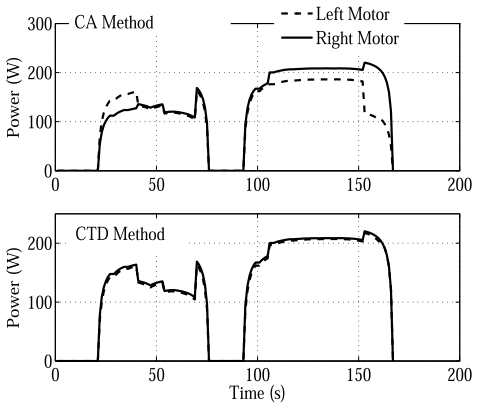

FIGURE 15. Traction power comparison using TA and CTD.

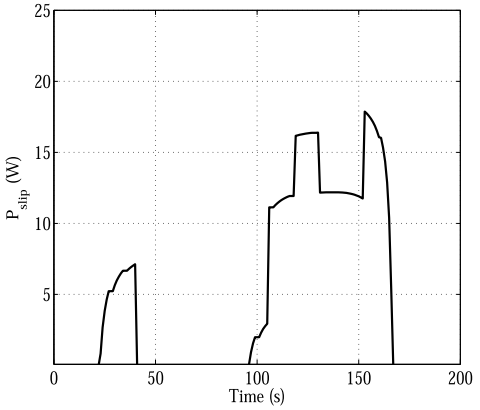

FIGURE 16. Difference of tire slip power dissipation between TA and CTD.

It shows that there is a significant improvement in power reduction by the use of the TA method. Another simulation is carried out to analyze the power dissipation due to wheel slip. In this analysis, it is observed that there is a significant power dissipation due to the wheel slip using CTD. This is because the CTD allocates the torque evenly irrespective of uneven wheel reaction force due to the occupancy variation. Hence, the extra motor energy is dissipated in the form of power loss due to wheel slip. Fig. 16 illustrates the difference in slip power dissipation due to CTD and TA methods. Additionally, the traction power consumption for both the driving wheels using TA is shown in Fig. 17. It shows that, the power consumption varies for different occupancy combinations. In addition to that, the average power consumption for a complete driving cycle is further illustrated in Fig. 18. Finally it can be concluded that the proposed method consumes less power compared to that of the conventional method.

It can be concluded that the overall power consumption comprises of two components: traction power and slip power. The traction power is proportional to the motor operating torque, speed and operating efficiency. Therefore, the traction power could be tuned by precisely tracking the motor efficiency map at a wide range of speed-torque values.

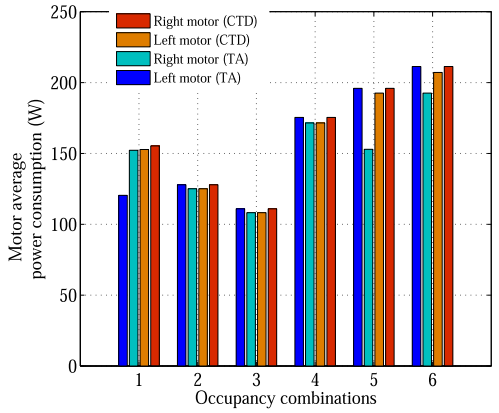

FIGURE 17. Traction power comparison for different occupancy payload combinations using TA and CTD.

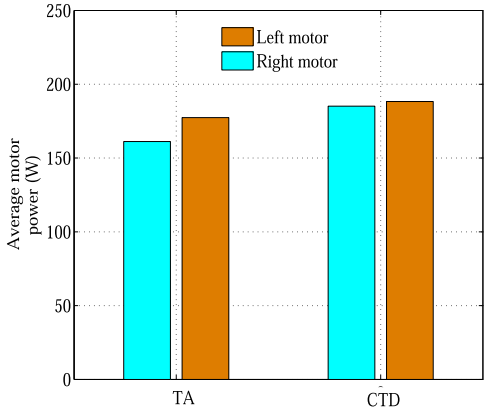

FIGURE 18. Traction power comparison for a complete driving cycle using TA and CTD.

However, the slip power dissipation requires including more detailed road tire interaction behaviour than that has been discussed in this work.

VII. CONCLUSION

In this paper, an energy-efficient TA model has been proposed for an LDEV having distributed drive-train configuration. It is based on the hypothesis that the passenger occupancy payload greatly influences the tractive effort needed to drive each vehicle's wheel. Therefore the TA scheme is proposed, limiting the excessive use of the driving power and reducing overall power dissipation. Optimal motor efficiency has been tracked via an optimization algorithm with the help of motor speed-torque characteristics and an efficiency map. In addition to that, a slip control method is proposed to reduce the wheel slip and the slip power dissipation. The overall model is established in the mathematical formulations and simulated using software simulation environment. Several simulations are conducted using IN-UDC. The outcome of the proposed scheme demonstrates the considerable improvement of the overall system efficiency as compared to the traditional method. The overall simulation results evince the feasibility and effectiveness of the proposed scheme. The model deals with simple mathematical formulations and hence it could be easy for real-time online implementations. There could be several opportunities for further improvements of the presented method. The real-time on-board implementation and validation of the proposed system will be the future direction of our work.

REFERENCES

[1] X. Zhang, D. Göhlich, and J. Li, "Energy-efficient toque allocation design of traction and regenerative braking for distributed drive electric vehicles," *IEEE Trans. Veh. Technol.*, vol. 67, no. 1, pp. 285–295, Jan. 2018.
[2] X. Jin, J. Wang, S. Sun, S. Li, J. Yang, and Z. Yan, "Design of constrained robust controller for active suspension of in-wheel-drive electric vehicles," *Mathematics*, vol. 9, no. 3, p. 249, Jan. 2021.
[3] Y. Chen and J. Wang, "Design and evaluation on electric differentials for overactuated electric ground vehicles with four independent in-wheel motors," *IEEE Trans. Veh. Technol.*, vol. 61, no. 4, pp. 1534–1542, May 2012.
[4] T. Zhu, X. Jin, G. Yin, J. Liang, and Z. Ren, "Coordinated control for active 4WS vehicle based on linear quadratic differential game," in *Proc. Chin. Control Decis. Conf. (CCDC)*, Jun. 2019, pp. 5478–5482.
[5] X. Ding, Z. Wang, and L. Zhang, "Hybrid control-based acceleration slip regulation for four-wheel-independently-actuated electric vehicles," *IEEE Trans. Transport. Electrific.*, vol. 7, no. 3, pp. 1976–1989, Sep. 2021.
[6] X. Ding, Z. Wang, L. Zhang, and C. Wang, "Longitudinal vehicle speed estimation for four-wheel-independently-actuated electric vehicles based on multi-sensor fusion," *IEEE Trans. Veh. Technol.*, vol. 69, no. 11, pp. 12797–12806, Nov. 2020.
[7] Z. Wang, C. Qu, L. Zhang, X. Xue, and J. Wu, "Optimal component sizing of a four-wheel independently-actuated electric vehicle with a real-time torque distribution strategy," *IEEE Access*, vol. 6, pp. 49523–49536, 2018.
[8] Y. Chen, S. Chen, Y. Zhao, Z. Gao, and C. Li, "Optimized handling stability control strategy for a four in-wheel motor independent-drive electric vehicle," *IEEE Access*, vol. 7, pp. 17017–17032, 2019.
[9] S. De Pinto, P. Camocardi, A. Sorniotti, P. Gruber, P. Perlo, and F. Viotto, "Torque-fill control and energy management for a four-wheel-drive electric vehicle layout with two-speed transmissions," *IEEE Trans. Ind. Appl.*, vol. 53, no. 1, pp. 447–458, Jan. 2017.
[10] N. J. Reza, *Vehicle Dynamics: Theory Application*. New York, NY, USA: Springer, 2014.
[11] X. Jin, J. Yang, Y. Li, B. Zhu, J. Wang, and G. Yin, "Online estimation of inertial parameter for lightweight electric vehicle using dual unscented Kalman filter approach," *IET Intell. Transp. Syst.*, vol. 14, no. 5, pp. 412–422, 2020.
[12] A. M. Dizqah, B. Lenzo, A. Sorniotti, P. Gruber, S. Fallah, and J. De Smet, "A fast and parametric torque distribution strategy for four-wheel-drive energy-efficient electric vehicles," *IEEE Trans. Ind. Electron.*, vol. 63, no. 7, pp. 4367–4376, Jul. 2016.
[13] Y. Suzuki, Y. Kano, and M. Abe, "A study on tyre force distribution controls for full drive-by-wire electric vehicle," *Vehicle Syst. Dyn.*, vol. 52, no. sup1, pp. 235–250, May 2014.
[14] R. Wang, Y. Chen, D. Feng, X. Huang, and J. Wang, "Development and performance characterization of an electric ground vehicle with independently actuated in-wheel motors," *J. Power Sources*, vol. 196, no. 8, pp. 3962–3971, 2011.
[15] H. Fujimoto and S. Harada, "Model-based range extension control system for electric vehicles with front and rear driving–braking force distributions," *IEEE Trans. Ind. Electron.*, vol. 62, no. 5, pp. 3245–3254, May 2015.
[16] Y. Chen and J. Wang, "Adaptive energy-efficient control allocation for planar motion control of over-actuated electric ground vehicles," *IEEE Trans. Control Syst. Technol.*, vol. 22, no. 4, pp. 1362–1373, Jul. 2014.
[17] A. Pennycott, L. De Novellis, A. Sabbatini, P. Gruber, and A. Sorniotti, "Reducing the motor power losses of a four-wheel drive, fully electric vehicle via wheel torque allocation," *Proc. Inst. Mech. Eng. D, J. Automobile Eng.*, vol. 228, no. 7, pp. 830–839, 2014.
[18] L. Zhang, Y. Wang, and Z. Wang, "Robust lateral motion control for in-wheel-motor-drive electric vehicles with network induced delays," *IEEE Trans. Veh. Technol.*, vol. 68, no. 11, pp. 10585–10593, Nov. 2019.

[19] Y. Chen and J. Wang, "Design and experimental evaluations on energy efficient control allocation methods for overactuated electric vehicles: Longitudinal motion case," *IEEE/ASME Trans. Mechatronics*, vol. 19, no. 2, pp. 538–548, Apr. 2014.
[20] C. Wang, Z. Wang, L. Zhang, D. Cao, and D. G. Dorrell, "A vehicle rollover evaluation system based on enabling state and parameter estimation," *IEEE Trans. Ind. Informat.*, vol. 17, no. 6, pp. 4003–4013, Jun. 2021.
[21] Y. Chen, X. Li, C. Wiet, and J. Wang, "Energy management and driving strategy for in-wheel motor electric ground vehicles with terrain profile preview," *IEEE Trans. Ind. Informat.*, vol. 10, no. 3, pp. 1938–1947, Aug. 2014.
[22] A. A. A. Ismail and A. Elnady, "Advanced drive system for DC motor using multilevel DC/DC buck converter circuit," *IEEE Access*, vol. 7, pp. 54167–54178, 2019.
[23] M. A. Obeidat, L. YiWang, and F. Lin, "Real-time parameter estimation of PMDC motors using quantized sensors," *IEEE Trans. Veh. Technol.*, vol. 62, no. 7, pp. 2977–2986, Sep. 2013.
[24] P. Podder, K. Das, S. Neroula, P. Barman, and S. Sharma, "Development of an automated setup for dynamic evaluation of DC motor characteristics," in *Proc. IEEE Calcutta Conf. (CALCON)*, Dec. 2017, pp. 190–195.
[25] O. Tremblay and L.-A. Dessaint, "Experimental validation of a battery dynamic model for EV applications," *World Electr. Vehicle J.*, vol. 3, pp. 289–298, May 2009.
[26] H. B. Pacejka, "Tyre brush model," in *Tyre and Vehicle Dynamics*, 2nd ed. Oxford, U.K.: Elsevier, 2005, pp. 93–134.
[27] Y. Chen and J. Wang, "A global optimization algorithm for energy-efficient control allocation of over-actuated systems," in *Proc. Amer. Control Conf.*, Jun. 2011, pp. 5300–5305.
[28] F. J. Perez-Pinal, I. Cervantes, and A. Emadi, "Stability of an electric differential for traction applications," *IEEE Trans. Veh. Technol.*, vol. 58, no. 7, pp. 3224–3233, Sep. 2009.
[29] B. Tabbache, A. Kheloui, and M. E. H. Benbouzid, "An adaptive electric differential for electric vehicles motion stabilization," *IEEE Trans. Veh. Technol.*, vol. 60, no. 1, pp. 104–110, Jan. 2011.
[30] G. A. Magallan, C. H. De Angelo, and G. O. Garcia, "A neighbourhood-electric vehicle development with individual traction on rear wheels," *Int. J. Electr. Hybrid Vehicles*, vol. 2, no. 2, pp. 115–136, 2009.
[31] M. U. Cuma and T. Koroglu, "A comprehensive review on estimation strategies used in hybrid and battery electric vehicles," *Renew. Sustain. Energy Rev.*, vol. 42, pp. 517–531, Feb. 2015.
[32] G. Cui, J. Dou, S. Li, X. Zhao, X. Lu, and Z. Yu, "Slip control of electric vehicle based on tire-road friction coefficient estimation," *Math. Problems Eng.*, vol. 2017, Nov. 2017, Art. no. 3035124.
[33] L. Zhang, Z. Wang, X. Ding, S. Li, and Z. Wang, "Fault-tolerant control for intelligent electrified vehicles against front wheel steering angle sensor faults during trajectory tracking," *IEEE Access*, vol. 9, pp. 65174–65186, 2021.
[34] G. A. Magallan, C. H. De Angelo, G. Bisheimer, and G. Garcia, "A neighborhood electric vehicle with electronic differential traction control," in *Proc. 34th Annu. Conf. IEEE Ind. Electron.*, Nov. 2008, pp. 2757–2763.
[35] J. L. F. Daya, P. Sanjeevikumar, F. Blaabjerg, P. W. Wheeler, and J. O. Ojo, "Implementation of wavelet-based robust differential control for electric vehicle application," *IEEE Trans. Power Electron.*, vol. 30, no. 12, pp. 6510–6513, Dec. 2015.
[36] A. Haddoun, M. E. H. Benbouzid, D. Diallo, R. Abdessemed, J. Ghouili, and K. Srairi, "Modeling, analysis, and neural network control of an EV electrical differential," *IEEE Trans. Ind. Electron.*, vol. 55, no. 6, pp. 2286–2294, Jun. 2008.

PRANJAL BARMAN received the M.Tech. and Ph.D. degrees from the Department of Electronics and Communication Engineering, Tezpur University, Assam, India, in 2013 and 2021, respectively. He is currently a Teaching Associate with the Department of Electronics and Communication Technology, Gauhati University, Assam. His research interests include electric vehicles, power electronics, and semiconductor device modeling and technology.

BRIAN AZZOPARDI (Senior Member, IEEE) received the B.Eng. degree from the University of Malta, in 2002, and the Ph.D. degree from The University of Manchester, U.K., in 2011. He is currently a Senior Academic with Malta College of Arts, Science and Technology (MCAST) and leads the Energy Research Group, and a Visiting Senior Lecturer with the University of Malta. His research interests include photovoltaics and electric mobility network integration and future urban low-carbon society.